Hindawi
Advances in Civil Engineering
Volume 2020, Article ID 8866621, 19 pages
https://doi.org/10.1155/2020/8866621

Research Article

Experimental Study of the Rock Mechanism under Coupled High Temperatures and Dynamic Loads

Huaming An,[1] **Tongshuai Zeng**,[1] **Zhihua Zhang**,[2] **and Lei Liu**[2]

[1]*Faculty of Public Security and Emergency Management, Kunming University of Science and Technology, Kunming 650093, China*
[2]*Faculty of Land Resources Engineering, Kunming University of Science and Technology, Kunming 650093, China*

Correspondence should be addressed to Lei Liu; explosive.lab@outlook.com

Received 14 March 2020; Revised 16 June 2020; Accepted 20 June 2020; Published 17 July 2020

Academic Editor: Zhiqiang Yin

With the development of modern society, geomaterials are widely used for infrastructure. These materials often experience dynamic loading and high temperature, which significantly influences the mechanical behaviour of the materials. This research focuses on the effects of the loading rate and high temperature on rock mass in terms of rock mechanism. A state-of-the-art review of rock mechanism under coupled dynamic loads and high temperatures is conducted first. The rock mechanism under static and dynamic loads is introduced. The marble is taken as the rock material for the test, while the split-Hopkinson pressure bar system is used to take the dynamic tests. In addition, the principles of the split-Hopkinson pressure bar are introduced to obtain the dynamic parameters. The fracture patterns of the uniaxial compressive strength test and the Brazilian tensile strength test are obtained and compared with those well documented in the literature. Some curves for the relationships among the loading rate, strain, temperature, compressive or tensile strengths are explained. It is conduced that with the increase of the loading rate, the rock strength increases, while with the increase of the temperature, the rock strength decreases.

1. Introduction

It is well known that the rock materials are widely used in many geostructures, such as foundations, tunnels, dam, and slops. However, the physical and chemical properties of the rock materials will be changed if they experience a high-temperature environment. This change will eventually affect the rock behaviours. In addition, rock mass in a deep tunnel or deep mine might be disturbed by explosion, earthquake, and sudden and natural disasters [1]. In this condition, the rock mass is experiencing an impact, i.e., dynamic loading. Although the dynamic behaviour of the rock mass has been intensively studied, the knowledge on the mechanism of the rock mass under dynamic loads is still limited us to a better understating of the dynamic behaviour of rock mass. Moreover, for rock mass under the coupled condition of high temperature and dynamic loading, the mechanism of rock failure will be more complicated. Thus, it is necessary to study the rock behaviour under coupled high temperatures and dynamic loading. To better understand the background of the study on the dynamic behavior of rock after heat treatment, a literature review is conducted in the following section. The main experimental equipment, i.e., split-Hopkinson pressure bar, is introduced [2, 3]. Then, static and dynamic tests for the rock after heat treatment are reviewed.

2. State-of-the-Art Review of Rock Mechanism under Dynamic Loads and High Temperatures

This section mainly reviews the rock fracture studies under high temperatures and dynamic loads. As the split-Hopkinson pressure bar (SHPB) is the most widely used technique to carry out the rock fracture mechanism under dynamic loads, the development of the technique is reviewed first. Then, many dynamic tests, such as the uniaxial compression test and Brazilian tensile strength test using SHPB, are reviewed. Among them, the influence of the loading rate

on the rock strength is intensively studied. After that, the rock mechanism under temperatures is reviewed. The review focuses on the physical properties of rock after high-temperature treatment and the static and the dynamic rock mechanism of rock under high temperature. Since the numerical studies of the dynamic rock fracture and fragmentation have been intensively studied and reviewed by the authors and more details can be found in the literature [4–14], the numerical studies of rock mechanism under high temperature are not reviewed herein.

2.1. Experimental Study of Rock Mechanism under Dynamic Loads

2.1.1. Development of the Split-Hopkinson Pressure Bar. As for the rock under dynamic loading, sources of dynamic loads could be explosion, impact, and seismic events [2, 3]. For research on the dynamic mechanism of rock, the split-Hopkinson pressure bar might be the most widely used technique [15–19]. Thus, the development of the split-Hopkinson pressure bar is introduced first. Kolsky used a pressure bar to test the pulse waveform, and it was the first time to measure the mechanical properties of rock under dynamic loads [20]. Kolsky improved the Hopkinson bar system, which is mainly divided into striker, incident bar, and transmission bar. As the system is comprised of several separated components, the system was called split-Hopkinson bar system [21]. Then, the system is used to study the rock mechanism at the strain rates within $10^1 \sim 10^4 S^{-1}$. Some of the brittle materials, such as rock, are heterogeneous and contain defects such as crack texture. Therefore, large enough materials are needed to reduce the impact of material's heterogeneity. As the size of the specimen increased, a larger diameter pressure bar was needed, so the large-diameter Hopkinson bar developed rapidly since the 1970s. The adoption of the large-diameter Hopkinson bar challenges the traditional theoretical assumptions of Hopkinson bar, i.e., one-dimensional stress wave hypothesis and uniform hypothesis. In addition, wave dispersion, stress unevenness, and cross section friction are the main problems needed to be solved for the large-diameter Hopkinson bar. The dispersion problem is caused by the ignorance of the inertia motion of particles in the Hopkinson bar with a large diameter [22]. For section friction, butter is generally applied to both ends of the specimen to reduce friction [22]. Moreover, since constant strain rate loading is very important for studying the constitutive relations under dynamic loads of rocks, many scholars have studied the realization of constant strain rate loading by the SHPB. For the first time, Samanta added a pad at the front end of the incident bar to realize constant strain rate loading [23]. The pad is made of the same material and size as the sample. Frew et al. pasted a copper sheet on the front end of impact bars to realize constant strain rate loading [24].

2.1.2. Rock Mechanism under Dynamic Loads. Most rock experiments techniques for carrying out the rock dynamic tests are developed from those techniques for static tests. At present, the standard dynamic experiment methods recommended by the international society of rock mechanics are uniaxial compression test, the Brazilian disk test, and semidisc with the prefabricated crack test. Tedesco et al. applied the Hopkinson pressure bar to conduct an impact test on cement and studied the influence of loading rate on cement strength [25]. Galvez et al. conducted impact tests on ceramic materials with the application of the Hopkinson pressure bar, and the study showed that the loading rates influence the tensile strength of the materials significantly [26]. Sukontasukkul et al. have studied the effect of loading rate on the damage of concrete using SHPB [27]. They concluded that the specimens subjected to impact loading were found to suffer higher damage than those subjected to static loading. Uniaxial and triaxial compressive strength tests have been conducted by Zhao, and the results showed that compressive strength will increase due to the increased loading rate [28]. Zhang et al. studied the influences of the loading rate on the rock fracture process and concluded that the number of cracks increases with the increasing loading rate [29]. Many researchers indicate the same conclusion that the loading rate significantly influences the behaviour of the brittle materials [27–34]. Wang et al. studied the fracture process of rock under high pressure by the Hopkinson pressure bar, and the study showed that the tensile strength and elastic modulus of rock under high strain rate were several times higher than those under static condition [35]. Dai et al. proposed a method for measuring dynamic mode-I rock fracture parameters using a cracked chevron notched semicircular bend (CCNSCB) specimen loaded by a split-Hopkinson pressure bar (SHPB) apparatus [31]. Zhou et al. studied the mechanical behaviour of rock under both dynamic and static loads from the theoretical and experimental perspectives [36]. The theoretical and experimental results show that when the stress wave front propagation is relatively slow, the disk can reach a stress equilibrium and the disk is split by the loading diameter [36]. When the force wave front is relatively fast, the Brazilian disk is not suitable for calculating the tensile strength of rock due to the uneven distribution of stress [36]. Mahanta et al. studied the effects of strain rate on fracture toughness and energy release rate of gas shales [33]. Peng used the split-Hopkinson pressure bar to conduct the Brazilian disc test and concluded that the time required to achieve a uniform stress state in specimen for the half-sine incident pulse is noticeably shorter than that for the perfectly rectangular incident pulse [37].

2.2. Experimental Study of Rock Mechanism under High Temperatures

2.2.1. Static Rock Mechanism under High Temperatures. In deep geotechnical engineering, such as deep mining, deep burial treatment of radioactive nuclear waste, coal gasification and exploitation, and utilization of geothermal resources, the physical and mechanical properties of rock are all affected by the high-temperature environment. Due to complex physical and chemical changes in the high-temperature environment, the physical and mechanical

behaviours of rock are different from those of normal temperature. Thus, the influence of temperature on rock mechanical properties has been widely studied worldwide. The influence of temperature on rock is mainly manifested in the following two aspects. On the one hand, the temperature field has an influence on the physical behaviour of rock. On the other hand, the change of thermodynamic parameters related to rock deformation affects the temperature field. On the contrary, the change of temperature field affects the mechanical properties of rock. Generally, when the temperature increases, the mechanical properties of the rock become weak, and the stiffness, compressive strength, tensile strength, elastic modulus, and other parameters of the rock will be reduced. At the same time, the increase of the temperature will also change the mineral composition of the rock, resulting in the increasing of the microfractures and joint fractures. Then, the study for physical property and the static rock mechanism under high temperature is reviewed as follows.

Van der Molen summarized the mechanical properties of rocks in high-temperature environments and analysed the changes of granite while it experiences high temperature under high confining pressure [38]. It is concluded that the porosity between the particles in the granite decreases when the temperature reaches 200°C, and the porosity between granite particles expands when the temperature is between 200°C and 840°C. Heard measured the thermal expansion coefficient and permeability of quartz, and the studies have shown that temperature has a significant effect on the thermal expansion coefficient of rocks. The higher the temperature, the higher the thermal expansion coefficient [39]. Yan studied the effects of high temperature on density, P-wave velocity, uniaxial compressive strength, and elastic modulus for granite, tuff, and breccia [40]. Fengchen studied the change law of the physical properties of sandstone with temperature and found that the bulk density of sandstone decreased with increasing temperature, and the porosity and permeability gradually increased with increasing temperature [41]. Zhao and Chen et al. studied the thermal expansion behaviour of limestone [42, 43]. It was found that the thermal expansion behaviour of limestone has a nonlinear relationship with temperature, and the porosity increases with temperature.

2.2.2. Dynamic Rock Mechanism under High Temperatures. During mining for deep resources, excavation for the deep tunnel by blasts, and gas explosion in mine coal, the underground rock mass is in the extreme environment of impact load and high temperature. Thus, it is essential to study the rock mechanism under dynamic loading and high temperature. Li used an experimental system with the function of coupling dynamic loads and high temperatures to carry out the rock behaviour test for siltstone and concluded that dynamic peak strength of siltstone increases with the increase of temperature in the range of 20°C–100°C and decreases with the increase of temperature when it exceeds 100°C [44].Yin carried out uniaxial dynamic compression experiments on sandstone cooled under the action of high temperature from room temperature to 800°C by using SHPB and analysed the change rule of rock density, longitudinal wave, and strength with temperature [45]. In addition, they also analysed the dynamic fracture characteristics of sandstone after high temperature from the failure form of sample and fragments. The results show that with the increase of temperature, the mechanical parameters such as density, P-wave velocity, and peak strength of the sample decrease gradually. Yin studied the dynamic mechanical properties of granite under the condition of temperature compression coupling. The results showed that the dynamic strength of granite decreased with the increase of temperature, while the peak strain increased with the increase of temperature [46]. Xu and Liu carried out impact compression experiments of marble at different temperatures and loading rates [47]. The results show that the peak strength and peak strain of marble increase with the increase of loading rate at different temperatures. When the temperature rises to 800°C, the peak strength of marble becomes less obvious with the change of loading rate The modulus decreases with the increase of temperature. When the temperature rises to 1000°C, the modulus of elasticity shows a basically constant trend with the increase of loading rate. Liu analysed the dynamic splitting tensile test of marble after high-temperature treatment and found that the tensile strength of marble after high-temperature treatment is significantly higher than that under static condition. Under the same impact pressure, the tensile strength of marble increases first and then decreases with the increase of temperature [48].

3. Materials and Methods

3.1. Preparation for the Rock Specimen. In this research, the marble from Gejiu Kafang tin mine in Yunnan Province of China is used to study the rock behaviour under the high temperatures and dynamic loads. The strata in the mining area are mainly divided into Triassic (t2 g) hydrochloride rock strata. The fold structure in the sampling area is mainly anticline, and the fault structure in the mining area is mainly east-west fault. The rock material is taken from the depth of 700 m in the mine. According to the geometry suggested by ISRM, the samples are made into cylinders with 50 mm in the diameter and 100 mm in length for the uniaxial compressive strength test under static loading. The sample with 40 mm in the diameter and 40 mm in length are made for the Brazilian tensile strength test under static loading and compressive strength test under dynamic loading.

3.2. Principles for the Rock Tests under Static Loads. Figure 1 depicts the geometrical model for the uniaxial compressive strength (UCS) test and the Brazilian tensile strength (BTS) test under static loads. For the UCS test as illustrated in Figure 1(a), it includes two loading plates under

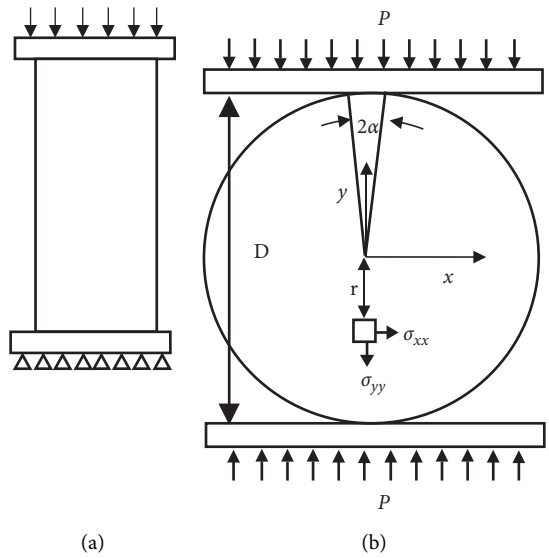

Figure 1: Geometrical model for UCS and BTS test. (a) Geometrical model for UCS test. (b) Geometrical model of BTS test.

the top and bottom of the rock specimen, while the sample is placed between the two loading plates. During testing, the two loading plates will move at a constant speed, as the loading plates contact the rock sample, the compressive stresses are produced immediately and propagate along the length of the specimen. After the stress increases and reaches the strength of the rock, fractures are produced. The compressive strength can be calculated according to

$$\sigma_c = \frac{P}{A}, \tag{1}$$

where P is the force on the top and bottom of the sample and A is the cross-sectional area of the top and bottom of the sample.

For the tensile strength test under static loading, the BTS test is used to obtain the tensile strength of the rock as illustrated in Figure 1(b). Since Akazawa and Carneiro [49, 50] developed the Brazilian disc test independently at almost the same time, the Brazilian disc test has gained its popularity for calculating the tensile strength and toughness. It is also widely used to study rock fracture initiation and propagation. Hondors [51] gave a complete stress solution for disc under diametral compression valid for both plane stress and plane strain conditions. This stress solution is then widely used to verify the numerical results of Brazilian disc test [52, 53].

Figure 1(b) shows the geometrical model of the BTS test. As shown in Figure 1(b), two plates are placed between the specimens. The two plates will move toward each other. The loads from the plates could be assumed to be radially applied over a short strip of the circumference with a radius of 2α, as shown in Figure 1(b). A complete stress solution along the loading diameter is given by Hondros as follows:

$$\sigma_{xx} = \frac{P}{\pi R t \alpha}\left\{\frac{\left[1-(r/R)^2\right]\mathrm{Sin}\,2\alpha}{1-2(r/R)^2\mathrm{Cos}\,2\alpha+(r/R)^4} - \tan^{-1}\left[\frac{1+(r/R)^2}{1-(r/R)^2}\tan(\alpha)\right]\right\}, \tag{2}$$

$$\sigma_{yy} = -\frac{P}{\pi R t \alpha}\left\{\frac{\left[1-(r/R)^2\right]\mathrm{Sin}\,2\alpha}{1-2(r/R)^2\mathrm{Cos}\,2\alpha+(r/R)^4} + \tan^{-1}\left[\frac{1+(r/R)^2}{1-(r/R)^2}\tan\alpha\right]\right\}, \tag{3}$$

where P is the applied load, R is the disc radius, r is the distance from the centre of the disc, t is the disc thickness, 2α is the angular distance of load arc, and σ_{xx} and σ_{yy} are the stresses along with the horizontal and vertical directions, respectively.

Thus, taking into account the specimen thickness t, the tensile strength can be calculated by (3) [54]:

$$\sigma_t = \frac{2P}{\pi Dt}, \tag{4}$$

where σ_t is the tensile strength, P is the applied load, and R is the diameter.

3.3. Principles of Split-Hopkinson Pressure Bar (SHPB). Figure 2 shows the conventional split-Hopkinson pressure bar (SHPB), which comprises a striker bar, an incident bar, and a transmission bar. The sample is placed between the incident and transmission bars during the dynamic experimental process. In the SHPB dynamic experiments, a gas

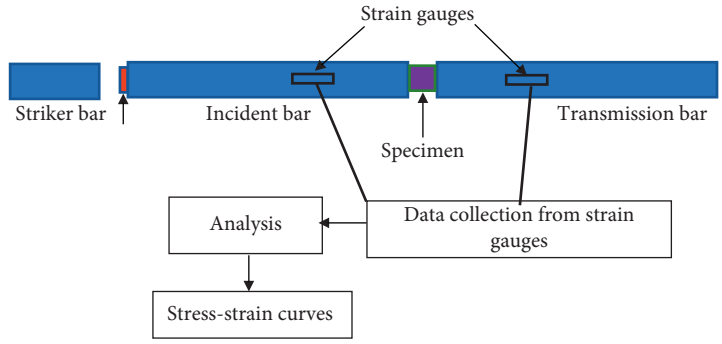

Figure 2: Schematic of conventional split-Hopkinson pressure bar (SHPB).

gun is used to launch the striker bar at the incident bar. Meanwhile, the elastic compression wave is produced to travel in the incident bar towards the sample. During the interaction between the striker bar and the sample, an elastic compression wave transmits into the transmission bar while an elastic tensile wave is reflected in the incident bar. It can be seen from Figure 2 that there are two strain gauges on the incident bar and the transmission bar. The incident strain pulse ε_i and reflected ε_r are measured by strain gauges on the incident bar, while the transmitted ε_t strain pulse is measured from the strain gauge on the transmitted bar.

Figure 3 shows the schematic diagram of the Hopkinson pressure bar during the dynamic test, and this diagram is used to explain the principle of the test. When the striker bar hits the incident bar, a compressive stress pulse wave of approximately one-dimensional propagation is generated in the incident bar. When the stress propagates to the interface where the incident bar and the transition bar are in contact (the 1-1 interface in Figure 3), a part of the compressive stress pulse wave continues to propagate into the sample, and the other part is reflected into the incident bar since the material of the sample is different from the incident bar in terms of wave impedance.

When the compressive stress pulse wave propagating into the rock sample reaches the contact surface of the sample and the transmission bar (the 2-2 interface in Figure 3), reflection and transmission are generated. A portion of the compressive stress pulse wave is reflected back into the sample at interface 2-2, while the other portion is transmitted into the transmission bar. When the compressive stress pulse wave is reflected back and forth for 3 to 6 times through the interfaces 1-1 and 2-2 in the rock sample, the stress equilibration is established in the rock sample.

In Figure 3, the cross-sectional area of the incident bar and the transmission bar is A_0. The cross-sectional area and length of the specimen are A and L. The stress at the interface of 1-1 is $\sigma_1(t)$, while the stress at the interface of 2-2 is $\sigma_2(t)$, and the stress of the specimen is $\sigma(t)$. The wave velocity and the elastic modulus of the incident bar and the transmission bar are C_0 and E_o, respectively, and the strain of the incident wave in the incident bar is ε_i and the reflected wave strain is ε_r. The transmission wave in the transmission rod is ε_t. The mass velocity at the interface of specimen 1-1 is u_1, and the particle velocity at the interface of specimen 2-2 is u_2. If the average strain in the specimen is ε, the strain rate is $\dot{\varepsilon}$. Based on the continuity condition of displacement and the one-dimensional stress hypothesis of stress wave, the following equations can be achieved.

Velocity on the interface1-1 is

$$u_1(t) = C_0[\varepsilon_i(t) - \varepsilon_r(t)]. \tag{5}$$

Velocity on the interface 2-2 is

$$u_2(t) = C_0\varepsilon_t(t), \tag{6}$$

Strain rate in the rock sample is

$$\dot{\varepsilon}(t) = \frac{u_1(t) - u_2(t)}{L} = \frac{C_0}{L}[\varepsilon_i(t) - \varepsilon_r(t) - \varepsilon_t(t)]. \tag{7}$$

Strain during time t is

$$D = f(\varepsilon, \dot{\varepsilon}). \tag{8}$$

Stress on 1-1 interface is

$$A\sigma_1(t) = A_0E_0[\varepsilon_i(t) + \varepsilon_r(t)]. \tag{9}$$

Stress on 2-2 interface is

$$A\sigma_2(t) = A_0E_0\varepsilon_t. \tag{10}$$

Average stress in specimen is

$$\sigma(t) = \frac{[\sigma_1(t) + \sigma_2(t)]}{2} = \frac{A_0E_0}{2A}[\varepsilon_i(t) + \varepsilon_r(t) + \varepsilon_t(t)]. \tag{11}$$

When the stress pulse wave propagates several times to and fro in the specimen, the stress equilibrium state is established. In this case, the three strains are equal as shown in equation (8):

$$\varepsilon_i + \varepsilon_r = \varepsilon_t. \tag{12}$$

Thus, by submitting (8) to (1)~(7), the following equations can be achieved:

$$\dot{\varepsilon}(t) = -\frac{2C_0}{L}\varepsilon_r(t), \tag{13}$$

$$\varepsilon(t) = -\frac{2C_0}{L}\int_0^t \varepsilon_r(t)\mathrm{d}t, \tag{14}$$

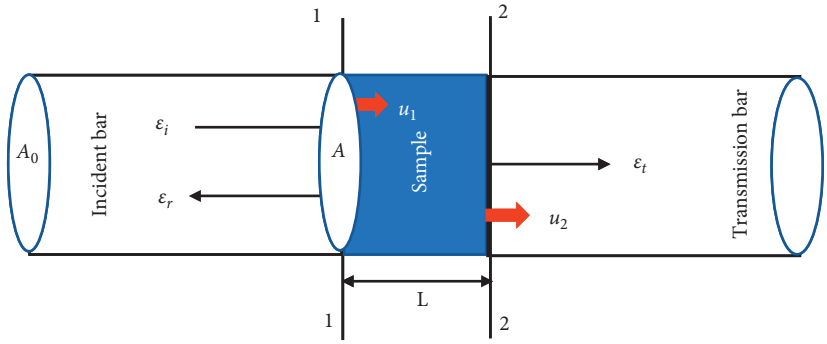

Figure 3: Schematic diagram of the rock sample under impact by SHPB.

$$\sigma(t) = \frac{A_0 E_0}{A}\varepsilon_t(t). \tag{15}$$

Equations (12)~(15) can be used to calculate stress, strain, and strain rate in the research.

4. Rock Behaviours under Static Loading with Various High Temperatures

In this research, a chamber-type electric resistance furnace (Figure 4) is employed to heat the rock sample to a specific temperature for testing the rock behaviour experiencing various high temperatures and under different loading rates. The temperatures are set as indoor temperature (25°C), 100°C, 200°C, 400°C, 600°C, and 800°C, respectively. Figure 5 illustrates the cooled and dried rock samples after experiencing the above high temperatures. As illustrated in Figure 5(a), the colour of the marble sample lightened to a certain extent after cooling at a temperature of 100°C~400°C, but the volume and surface flatness did not change significantly. After experiencing the high temperature of 600°C, the colour of the rock gradually turns gray and white, and the surface flatness changes slightly. At 800°C (Figure 5(b)), the colour changes significantly, i.e., the marble turns white. Moreover, the volume of the specimen expands and obvious cracks appear. In addition, the surface of the specimen becomes very rough. This indicates that the specimen is damaged under the action of temperature and the internal structure of the rock has undergone obvious deterioration.

4.1. Uniaxial Compressive Strength (UCS) Test. As illustrated in Figure 6, YAW-2000 computer-controlled automatic pressure testing machine is used to carry out the UCS test and BTS test under static loads. In order to mitigate the end effects due to the frictions initiating from the two loading contacts, i.e., contacts of the sample ends and the loading plates, some lubricating oil is placed on the loading contacts. At the beginning of the testing, the loading plate is moving at a speed of 0.002 $\text{mm} \cdot \text{s}^{-1}$. After the loading plate contacts the specimen, the loading plate is then applying the load of $1\,\text{kN} \cdot \text{S}^{-1}$ to the specimen until the specimen fails.

The averages of the rock parameters obtained from the test are recorded in Table 1, while Figure 7 shows the rock fracture patterns of the UCS test for those specimens under

Figure 4: XH7L chamber-type electric resistance furnace.

different temperatures. From the indoor temperature to 600°C, the rock fracture patterns are not significantly changed as the temperature increases. The rock mainly fractures along an inclined line or the vertical line which demonstrated typical characteristics of brittle materials under compression. According to the numerical study of the rock fracture process in the UCS test by a hybrid finite-discrete element method, the fractures are a mix of mode I-II damage (Figure 7(h)), i.e., mixed pure mode I fracture (Figure 7(g)) and pure mode II fracture.

Table 1 lists the obtained average compressive strength, strain on the vertical direction, and the Young modulus. The three parameters are significantly influenced by the increase of the temperature. With the increase of the temperature, those three parameters decrease significantly.

Figure 8 illustrates the stress-strain curves for those rock samples under various temperatures, while in general, as illustrated in Figure 8, the shape of the stress-strain curve is roughly the same, and each curve has experienced four stages: compaction stage, elastic stage, plastic deformation

(a) (b)

Figure 5: Rock sample for uniaxial compressive strength test after undergoing various temperatures. (a) Rock sample after experiencing the temperature from 25°C to 600°C. (b) Rock sample after undergoing 800°C.

Figure 6: YAW-2000 computer-controlled automatic pressure testing machine.

Table 1: Rock parameters obtained from the uniaxial compressive test under various temperatures.

Temperature (°C)	Compressive strength σ (MPa)	Strain ε (10^{-3})	Young's modulus E (GPa)
25	80.6	2.12	34.7
100	74.5	2.15	31.8
200	65.4	4.03	29.6
400	48.3	5.92	22.93
600	49.6	11.2	19.34
800	34.2	14.64	4.6

stage, and failure stage. In other words, the overall change trend for each curve is the same. When the marble temperature increases gradually, the slope of the compaction stage, i.e., the straight line of each curve, decreases, which indicates that the elastic modulus decreases with the increase of the temperature. This trend is confirmed by the elastic modulus in Table 1. For the specimen under the high temperature beyond 400°C, the peak stress of the rock decreases obviously, and the time to reach the peak stress increases, which indicates that the temperature has a great influence on the strength of the rock. As the temperature of the specimen increases gradually, the axial strain tends to increase, which is mainly due to the weakening and ductility of the material brittleness. By comparing the stress-strain whole-process curves in the above temperature ranges, it can be seen that with the increase of temperature, the brittleness, ductility, and peak strength of the rocks decrease. The curves still show the characteristics of brittle material failure process.

Figure 9 shows the relationship between the uniaxial compressive strength and the temperature. The temperatures have a significant impact on the strength of the rock. As can be seen from Figure 9, the strength of the rock decreased significantly from approximately 78 MPa to 20 MPa with the increase of the temperature from the indoor temperature to 800°C.

4.2. Brazilian Tensile Strength Test. Figure 10 illustrates the fracture patterns for the BTS test under different temperatures. The specimens mainly fracture along the loading diameter, and the main fractures separate the specimen into two halves. The fracture pattern is not significantly influenced by temperature.

Table 2 gives the tensile strength of the rock under different temperatures, while Figure 11 illustrates the corresponding curve.

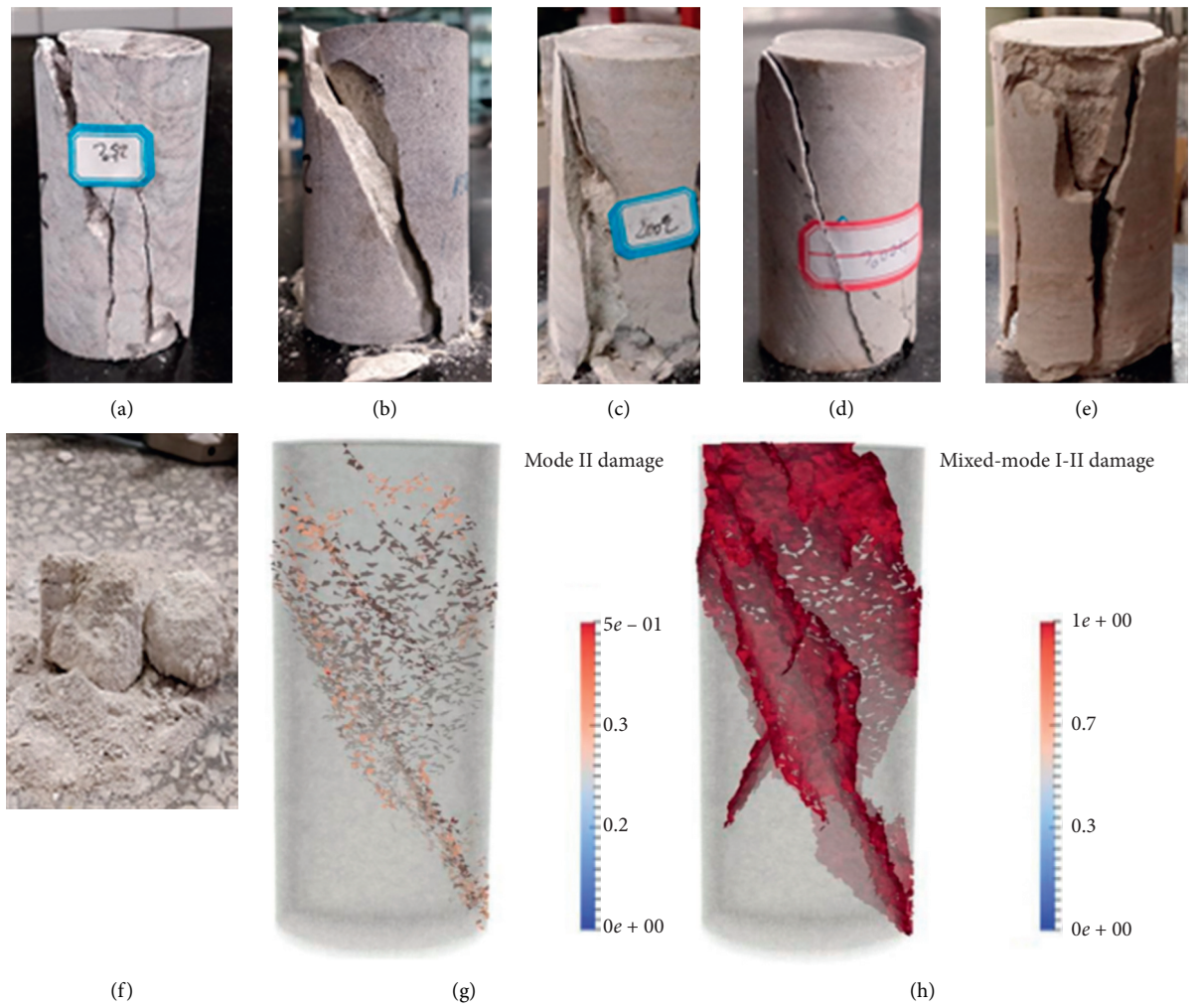

Figure 7: Fracture patterns for the UCS test under different temperatures: (a–f) experimental results; (g) mode II damage [55]; and (h) mixed-mode I-II damage [55]. (a) 25°C. (b) 100°C. (c) 200°C. (d) 400°C. (e) 600°C. (f) 800°C.

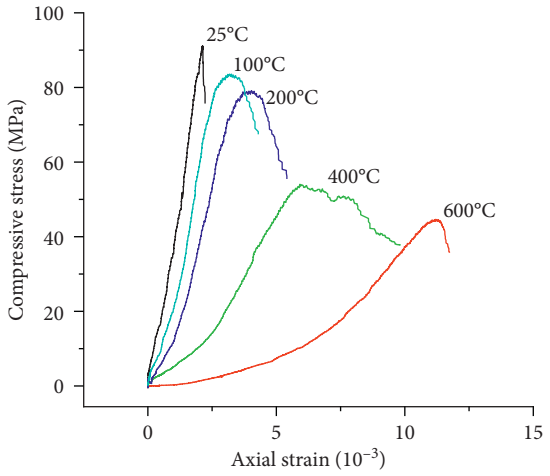

Figure 8: Stress-strain curve for uniaxial compressive strength test.

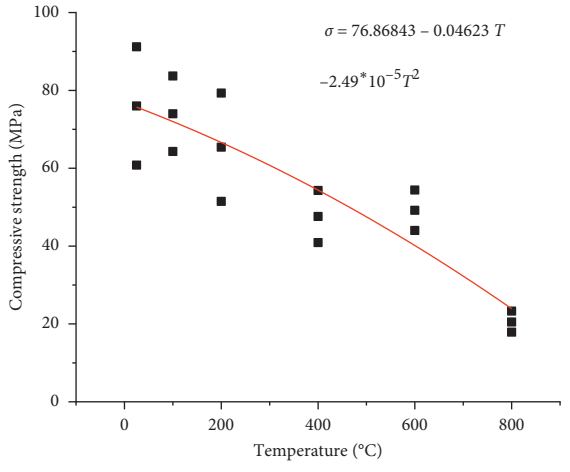

Figure 9: The strength-temperature curve for uniaxial compressive strength test.

As shown in Figure 11, the average results of static splitting tensile strength experiments show that the splitting tensile strength of marble at each temperature has a large dispersion. In general, the splitting tensile strength of marble is 6.98 MPa at room temperature. After that, the tensile strength kept floating around 6.5 MPa until it reached about

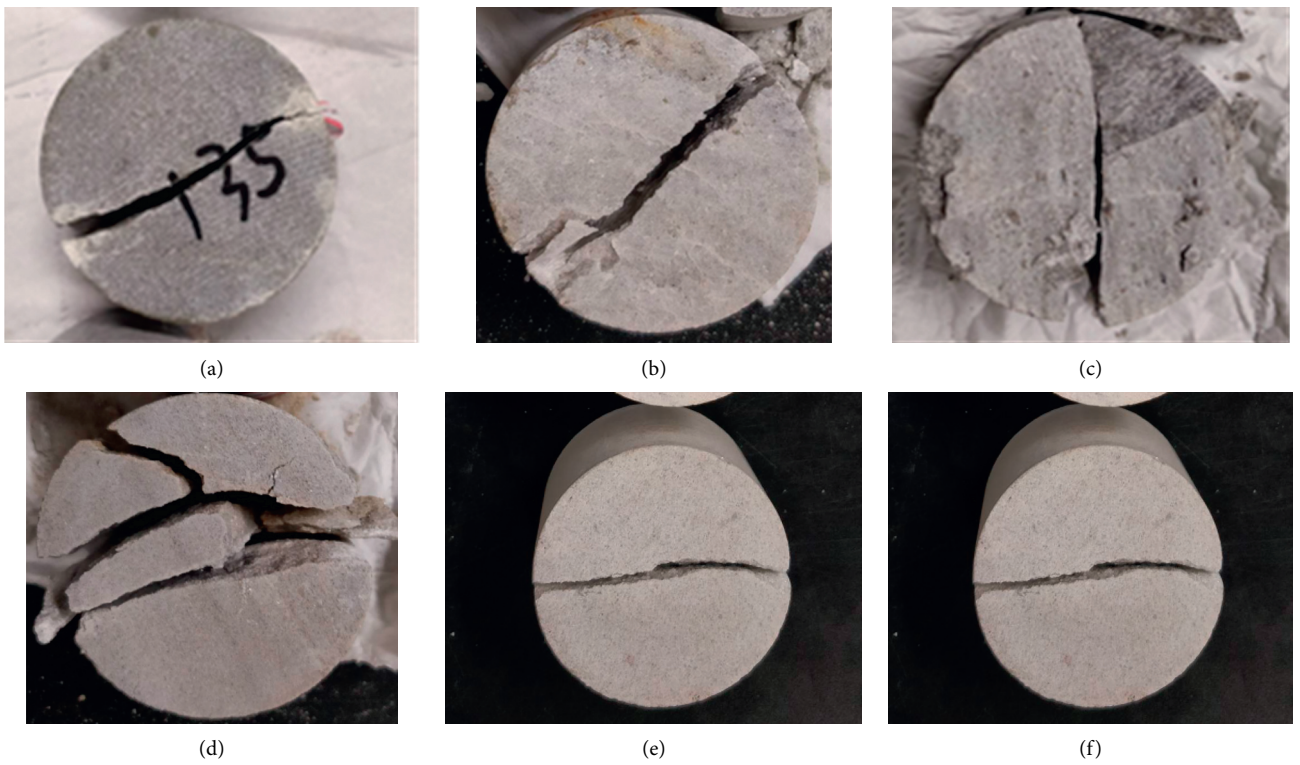

Figure 10: Rock fracture patterns for BTS test under various temperatures. (a) 25°C. (b) 100°C. (c) 200°C. (d) 400°C. (e) 600°C. (f) 800°C.

Table 2: Tensile strengths of the rock under different temperatures.

Temperature (°C)	25	100	200	400	600	800
Tensile strength σ (MPa)	6.82	6.64	6.44	6.8	6.48	3.4

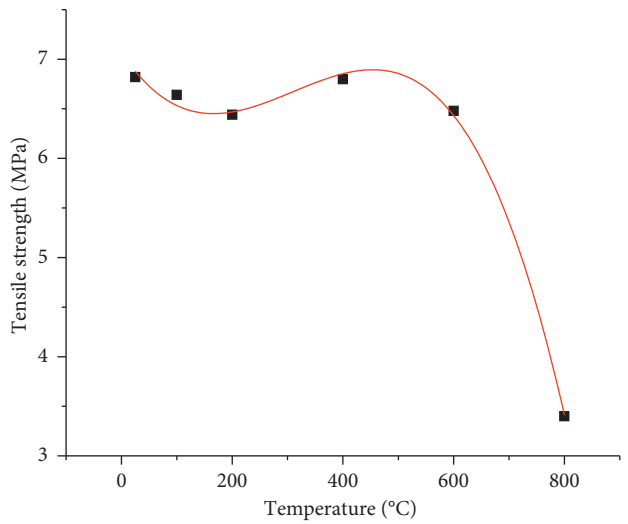

Figure 11: Tensile strength of the marble under different temperatures.

600°C. For the temperature of 800°C, the tensile strength of marble is only 3.40 MPa, about 43% decrease compared that at room temperature.

5. Rock Behaviours under Dynamic Loading and Different Temperatures

Figure 12 illustrates the HSPB system used for dynamic rock behaviour tests. The main components are gas gun, striker, incident bar, transmission bar, and dynamic strain meter system. Firstly, the striker is accelerated by gas gun to impact one end of the incident bar. Then, a dynamic compressive strain wave is induced in the incident bar and propagates toward the other end of the incident bar. Some portion of the compressive strain wave will be reflected at the interface between the incident bar and the specimen, and the reflected wave will turn into a tensile wave. The remaining portion will propagate into the specimen still as compressive strain wave. As the transmitted compressive strain wave reaches the interface of the specimen and the transmission bar, the disk is subjected to dynamic loading.

The rock material for the dynamic compression strength is the same as that used for the static test in the last section. The diameter of the cylinder is 50 mm, while the length is 40 mm. The temperature gradient of this experiment is divided into six degrees, i.e., 25°C, 100°C, 200°C, 40°C, 600°C, and 800°C. The heating rate of the resistance furnace is set as 10°C/min. When the temperature reaches the prescribed temperature, it is then heated at a constant temperature for another three hours to obtain marble samples under uniform high temperature. Then SHPB experiment under high temperature is carried out. In the experiment, impact speed is set as 10 m/s, 12.5 m/s, and 14.5 m/s, respectively.

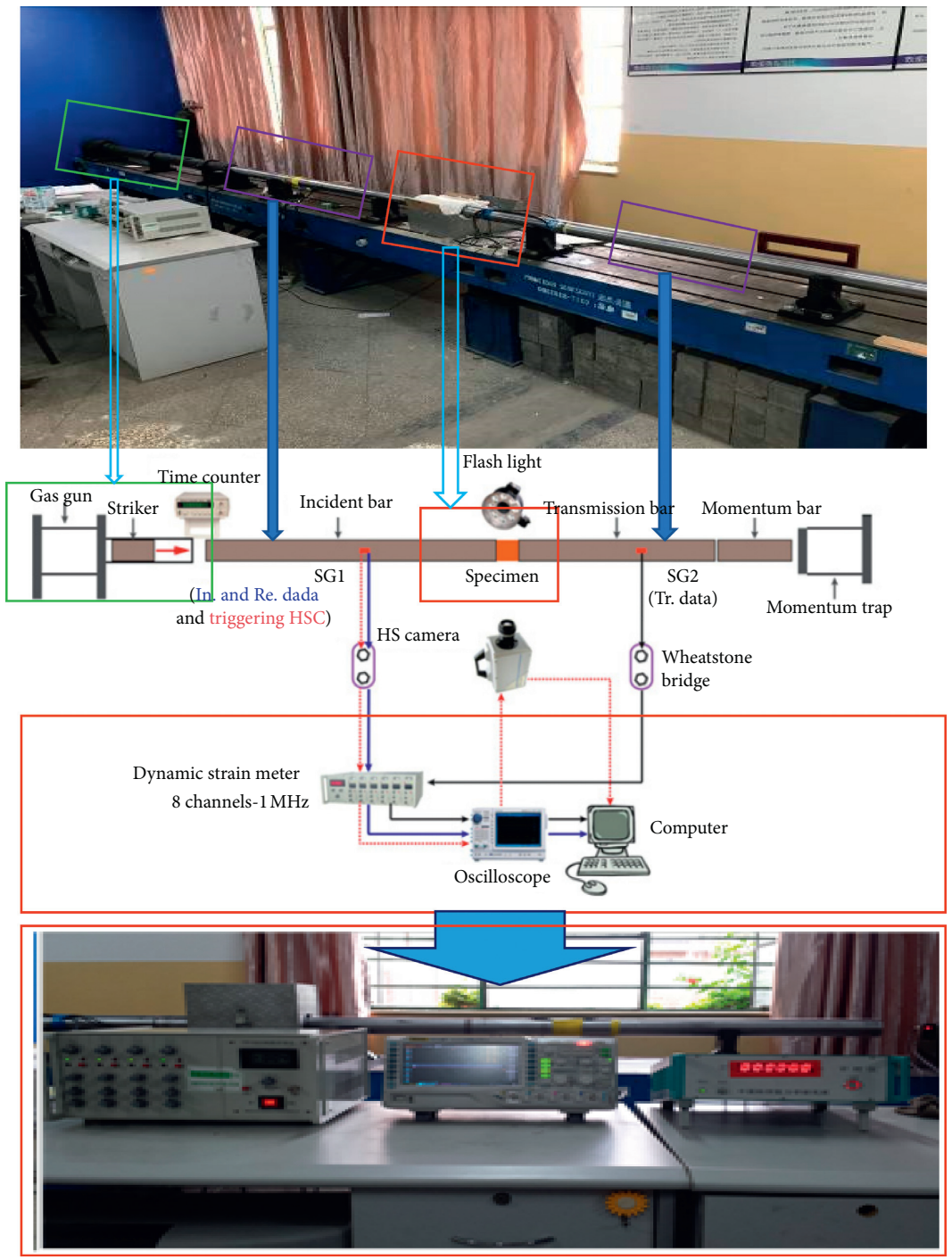

Figure 12: SHPB system (the schematic of the SHPB is adopted from Zhang and Zhao (2013) [56]).

5.1. Dynamic Uniaxial Compressive Strength (UCS) Test for Rock Specimens under Various Temperatures. Figure 13 illustrates the fragments produced by the dynamic UCS test. The strain rate significantly influences the test results in terms of the fragment size and size distribution. The larger the strain rate is, the finer the fragments produced for the specimen under the same temperature are. In addition, with the temperature increases, the size of the fragments decreases under the same loading rate.

Table 3 shows the influences of the impact strain rate, peak stress, peak strain, and Young's modulus by the impact speed and the temperature. In general, for a specific temperature, with the increase of the impact speed, the strain rate, peak stress, peak strain, and Young's modulus also increase. On the contrary, for a specific impact speed, with the increase of the impact speed, the strain rate increases, while the peak stress, peak strain, and Young's modulus decreases. More details for the relationship among those parameters are analysed from Figures 14–18.

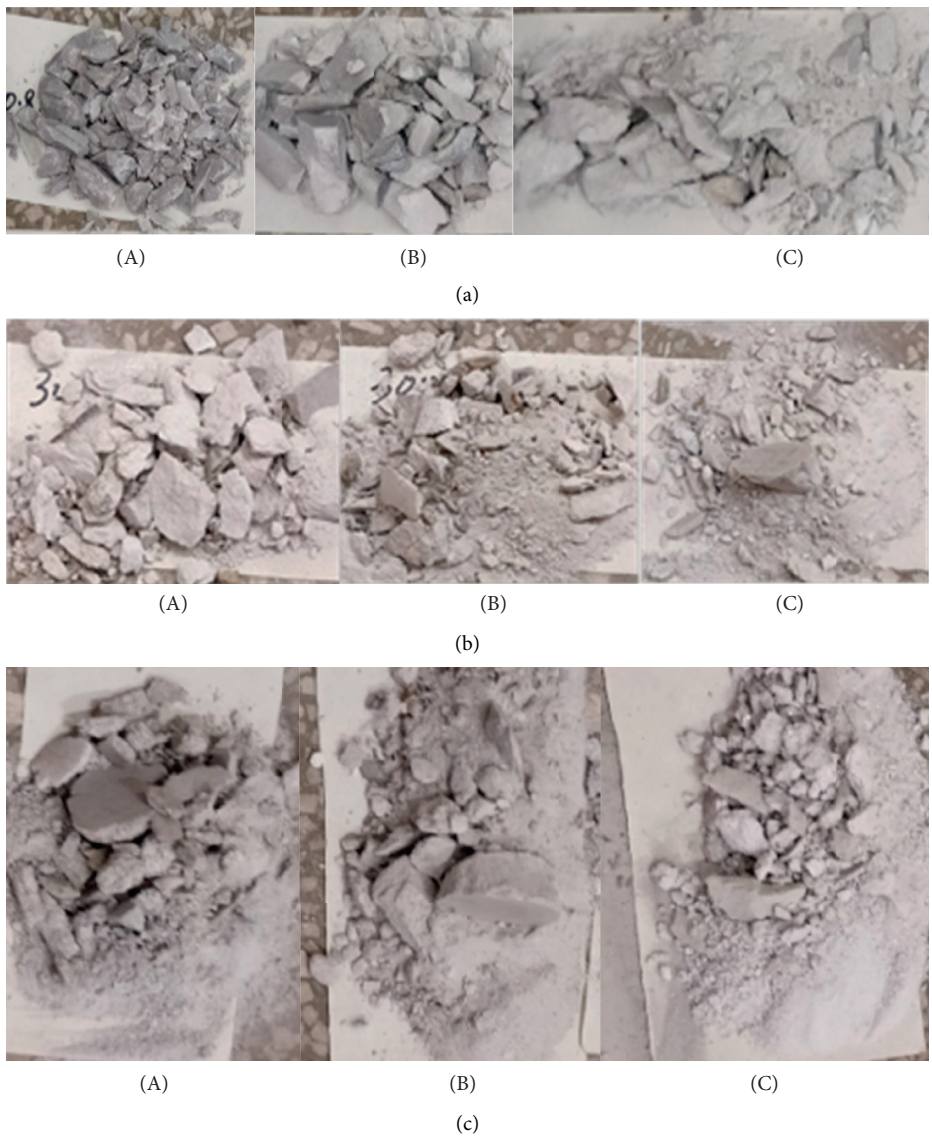

Figure 13: Rock fragments produced by the UCS test under coupled temperatures and strain rates. (a) I 25°C: (A) 84.7 s^{-1}, (B) 87.1 s^{-1}, and (C) 127.8 s^{-1}. (b) II 400°C: (A) 104.7 s^{-1}, (B) 07.1 s^{-1}, and (C) 137.8 s^{-1}. (c) III 600°C: (A) 200.7 s^{-1}, (B) 217.1 s^{-1}, and (C) 57.8 s^{-1}.

Figure 14 illustrates the stress-strain curves for the rock under different impact speed and temperatures. All the curves show a typical brittle rock failure process. Take the curves under the temperature of 25°C as an example (Figure 14(a)). The curves could be divided into four stages:

(i) OA: as the strain increases, the existing microfractures are closed. The duration of this stage is very short.

(ii) AB: the stage of AB is considered as linear elastic and deformation is fully recoverable.

(iii) BD: the stage of BD is the nonlinear elastic stage. During this stage, the fracture propagates stably. If the load is removed, the fracture propagation will be stopped.

(iv) DF: DF is the unstable fracture propagation stage. D is the yielding point, and beyond this point, the permanent deformation develops and it is not recoverable even if the load is removed.

Compared with those figures (Figures 14(a)–14(f)), all the curves demonstrate the same trend although under various loading rates and high temperature. For an individual figure in Figure 14, it is indicated that with the increase of the loading rate, the rock strength increases. Compared with curves in different figures, it is indicated that with the increase of the temperature, the rock strength decreases.

Since the peak stress, peak strain, and Young's modulus of the brittle materials are significantly influenced by the strain rates and the temperature, relationships among them are discussed according to Figures 15–17. As illustrated in Figures 15 and 16, with the increase of temperature, the peak stresses of the rock specimens under three different impact speeds decrease dramatically (Figure 15), while with the

Table 3: Parameters obtained during the dynamic compressive strength tests.

Temperature T (°C)	Impact speed V (m/s)	Strain rate $^{*}\varepsilon$ (s^{-1})	Peak stress σ_d (MPa)	Peak strain ε_d (10^{-3})	Young's modulus E_c (GPa)
	10.0	96.09	199.73	3.56	25.39
25	12.5	108.44	224.68	4.15	33.10
	14.5	117.90	246.70	11.25	36.00
	10.0	100.12	191.14	1.77	33.21
100	12.5	108.08	196.26	6.87	30.02
	14.5	118.08	205.76	8.99	31.96
	10.0	118.70	152.99	3.05	34.56
200	12.5	122.44	168.14	8.1	30.73
	14.5	135.93	240.71	12.91	28.68
	10.0	122.63	146.69	6.02	29.86
400	12.5	139.37	161.15	8.48	15.44
	14.5	161.25.	213.27	11.38	23.12
	10.0	135.29	85.16	6.42	5.48
600	12.5	160.19	104.29	9.96	12.26
	14.5	174.05	151.90	13.7	13.50
	10.0	206.78	33.00	8.14	1.92
800	12.5	215.47	35.91	18.03	2.63
	14.5	222.66	59.44	18.87	3.48

increase of the strain rate, the peak stresses increase fast (Figure 16). The relationship between dynamic peak stress and temperature change of marble specimens at different impact velocities can be fitted as shown in the following equations:

$$\begin{aligned}
10.0\,\text{m/s}\ \sigma &= -0.28\left(\frac{T}{100}\right)^3 + 2.5\left(\frac{T}{100}\right)^2 - 23.4\left(\frac{T}{100}\right) \\
&\quad + 205.72 \quad R^2 = 0.978, \\
12.5\,\text{m/s}\ \sigma &= -0.73\left(\frac{T}{100}\right)^3 + 7.77\left(\frac{T}{100}\right)^2 - 40\left(\frac{T}{100}\right) \\
&\quad + 230.85 \quad R^2 = 0.986, \\
14.5\,\text{m/s}\ \sigma &= -0.24\left(\frac{T}{100}\right)^3 + 0.85\left(\frac{T}{100}\right)^2 - 0.06\left(\frac{T}{100}\right) \\
&\quad + 240.20 \quad R^2 = 0.989.
\end{aligned} \tag{16}$$

Figure 17 illustrates the peak strain-temperature curves of rock under different impact loads. In general, with the increase of the temperatures, the peak strains increase. For the impact velocity of 10 m/s, the peak strain increases almost linearly. For the impact velocities of 12.5 m/s and 14.5 m/s, the peak strains increase fast when the temperature is beyond 400°C.

The relationship between the dynamic peak strain of marble specimen under different impact velocities and the change of temperature can be fitted as follows:

$$\begin{aligned}
10.0\,\text{m}\cdot\text{s}^{-1}\ \sigma &= -8.76\left(\frac{T}{1000}\right)^3 + 10.4\left(\frac{T}{1000}\right)^2 + 4\left(\frac{T}{1000}\right) \\
&\quad + 2.64 \quad R^2 = 0.959, \\
12.5\,\text{m}\cdot\text{s}^{-1}\ \sigma &= 119.56\left(\frac{T}{1000}\right)^3 - 130.45\left(\frac{T}{1000}\right)^2 \\
&\quad - 46.43\left(\frac{T}{1000}\right) + 3.18 \quad R^2 = 0.999, \\
14.5\,\text{m}\cdot\text{s}^{-1}\ \sigma &= 42.54\left(\frac{T}{100}\right)^3 - 34.13\left(\frac{T}{1000}\right)^2 \\
&\quad - 10.91\left(\frac{T}{1000}\right) + 10.19 \quad R^2 = 0.871.
\end{aligned} \tag{17}$$

Figure 18 illustrates the relationship between Young's modulus and the temperature under three different impact velocities. Before 200°C, with the increase of the temperature, Young's modulus is not influenced. However, after 200°C, Young's modulus decreases dramatically.

The relationship between the dynamic modulus of elasticity of marble specimens with different impact velocities and the change of temperature can be fitted as follows:

$$\begin{aligned}
10.0\,\text{m}\cdot\text{s}^{-1}\sigma &= 0.41\left(\frac{T}{100}\right)^3 - 5.89\left(\frac{T}{100}\right)^2 + 18.49\left(\frac{T}{100}\right) \\
&\quad + 20.34 \quad R^2 = 0.975,
\end{aligned} \tag{18}$$

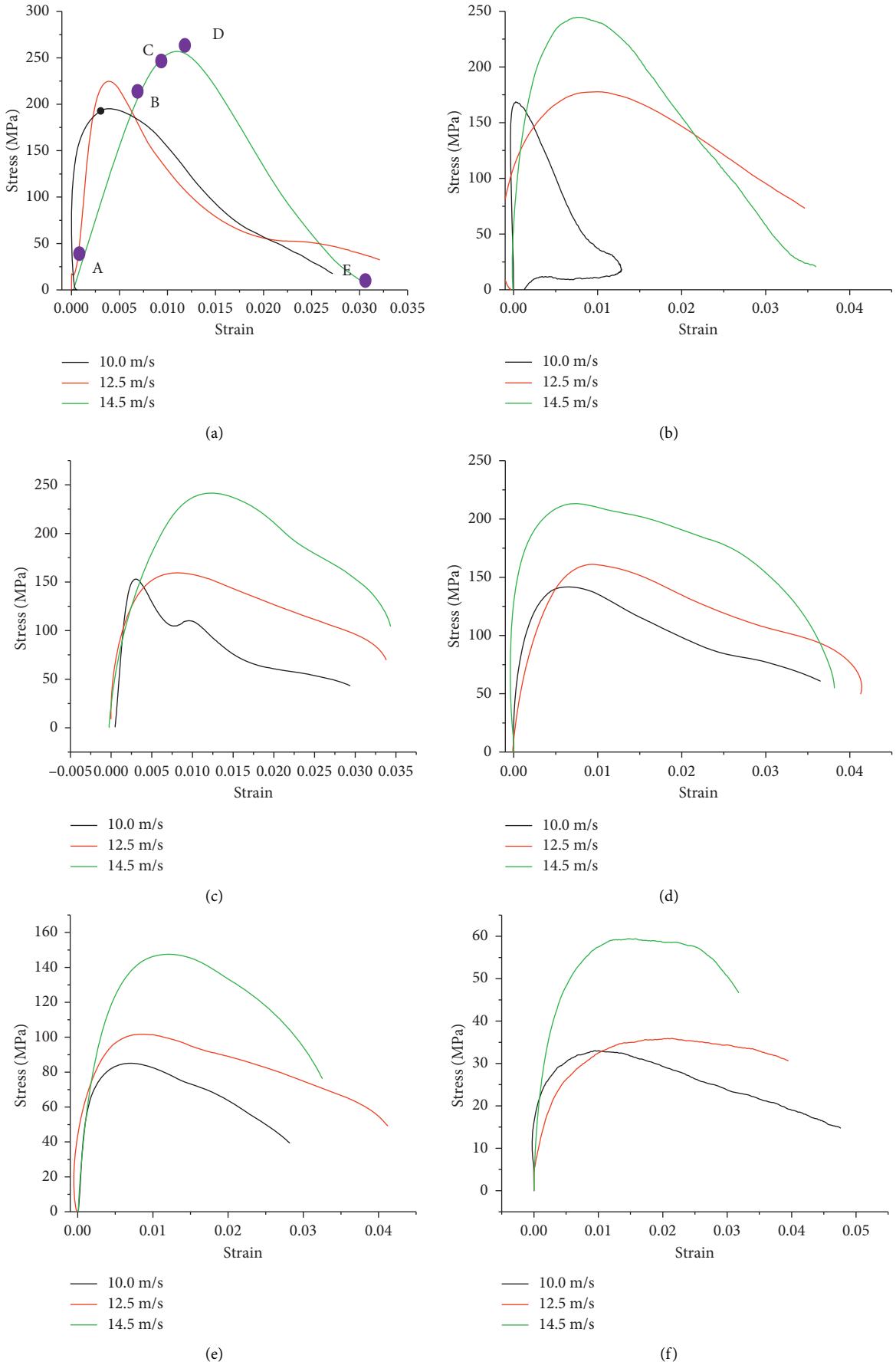

Figure 14: Stress-strain curves of rock under different impact speeds and different temperatures. (a) 25°C. (b) 100°C. (c) 200°C. (d) 400°C. (e) 600°C. (f) 800°C.

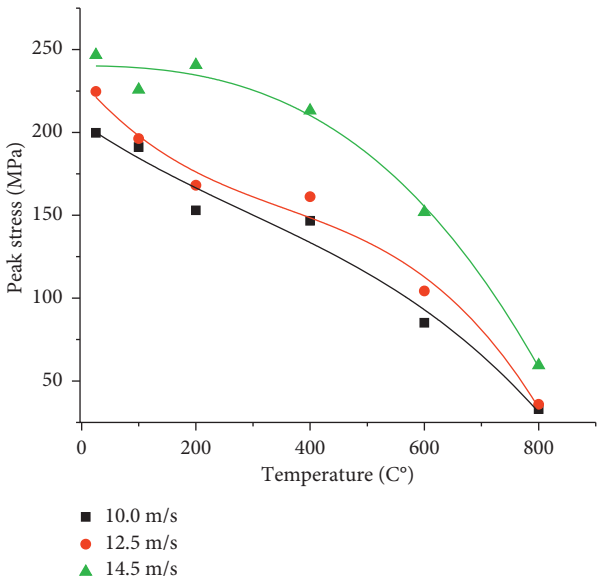

Figure 15: Peak stress-temperature curves of rock under different impact speeds and different temperatures.

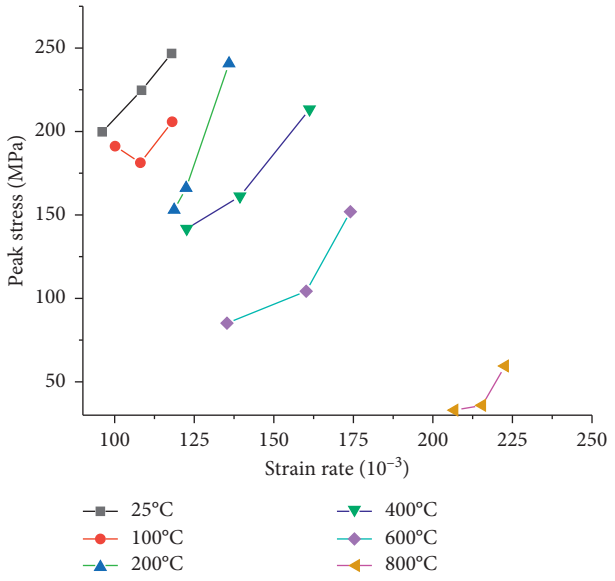

Figure 16: Peak stress-strain rate curves of rock under different impact speeds and different temperatures.

$$12.5\,\mathrm{m}\cdot\mathrm{s}^{-1}\ \sigma = 0.043\left(\frac{T}{100}\right)^3 - 53.50\left(\frac{T}{100}\right)^2 - 2.29\left(\frac{T}{100}\right) + 33.92 \quad R^2 = 0.963, \tag{19}$$

$$14.5\,\mathrm{m}\cdot\mathrm{s}^{-1}\ \sigma = -0.039\left(\frac{T}{100}\right)^3 + 0.33\left(\frac{T}{100}\right)^2 - 4.29\left(\frac{T}{100}\right) + 36.58 \quad R^2 = 0.997. \tag{20}$$

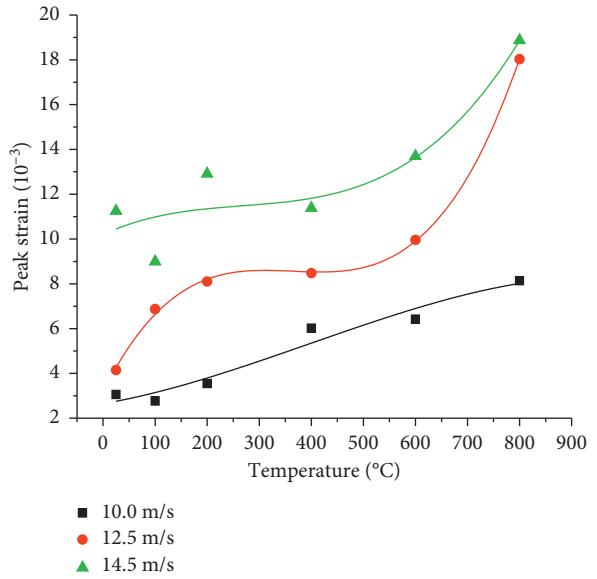

Figure 17: Peak strain-temperature curves of rock under different impact speeds and different temperatures.

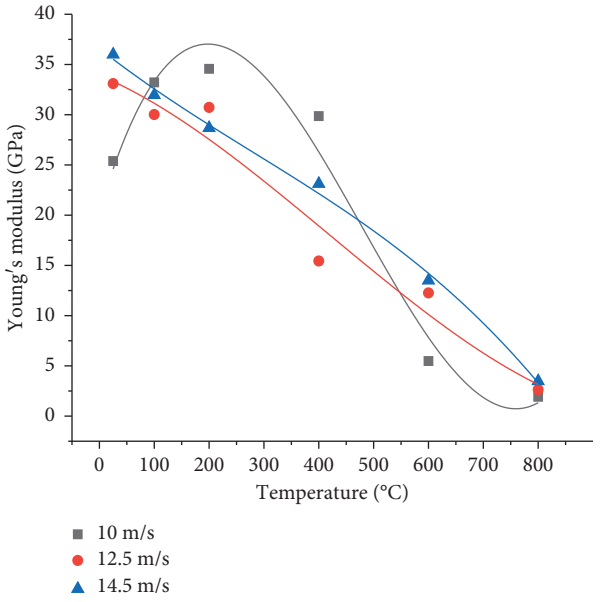

Figure 18: Young's modulus-temperature curves of rock under different impact speeds and different temperatures.

5.2. Dynamic Tensile Strength Test for Rock Specimens under Various Temperatures. For the dynamic tensile strength test, the impact velocities for bullet are 5 m/s, 7 m/s, and 9 m/s, respectively. The temperatures for rock specimens are still set as 25°C, 100°C, 200°C, 40°C, 600°C, and 800°C. The specimen cylinder for the dynamic BTS test is prepared with a diameter of 50 mm and a height of 40 mm. The signals obtained by SHPB during the dynamic test can be processed by (12)–(14).

Figure 19 illustrates the rock fracture process during the dynamic BTS test. As can be seen from Figure 19 under

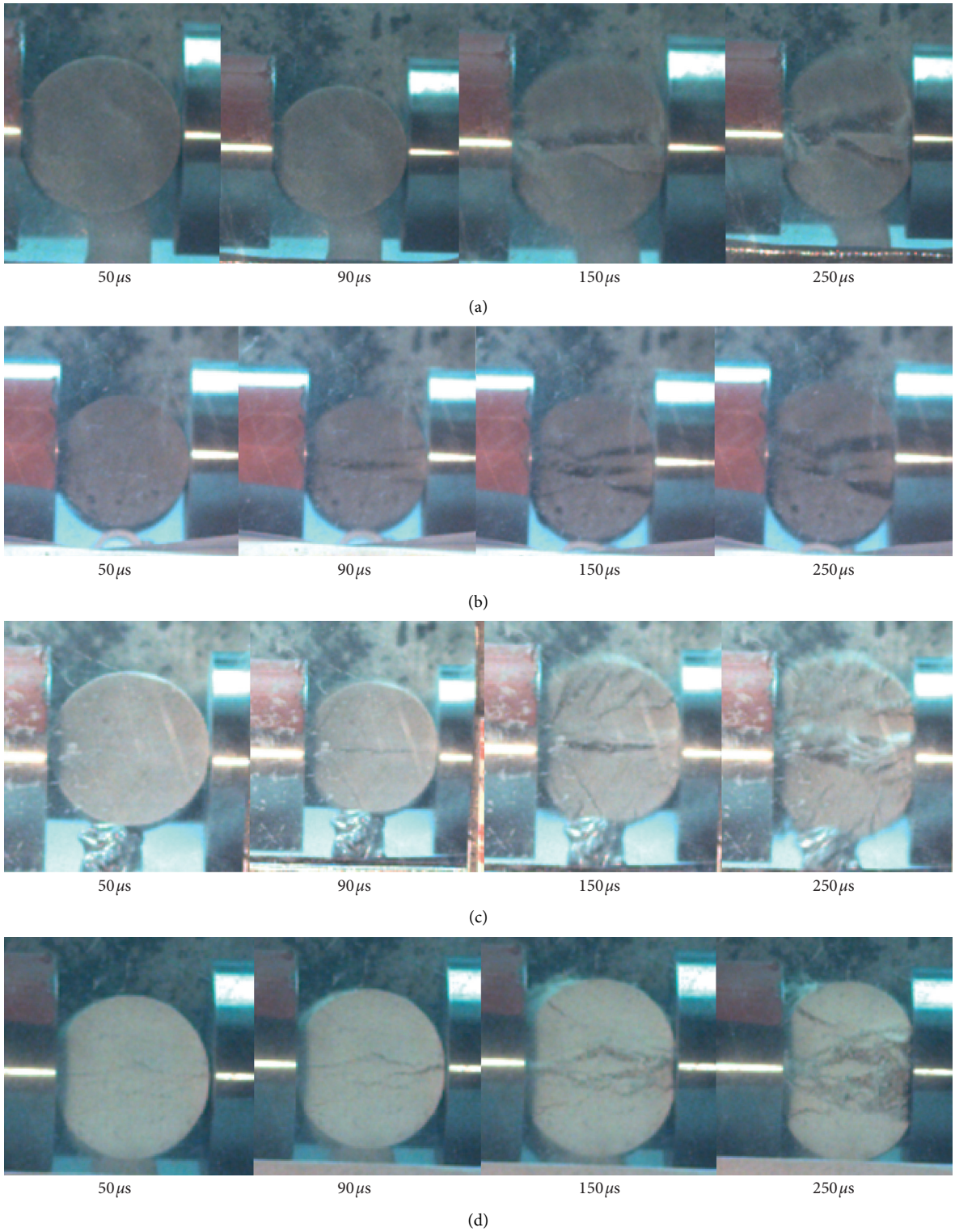

Figure 19: Failure process of marble under temperature from 200°C to 800°C obtained by a high-speed camera. (a) 200°C. (b) 400°C. (c) 600°C. (d) 800°C.

various temperatures, in the process of marble failure under different temperature conditions under high strain rate, the marble specimen first breaks into two parts along the radial (impact loading) direction, accompanied by a small amount of debris. In addition, some secondary cracks are produced at the loading end, forming a nearly triangular fragmented block. With the increase in temperature, the area of triangular breakage increases gradually. With the increase of the temperature, the fragments produced by the impact loading increase.

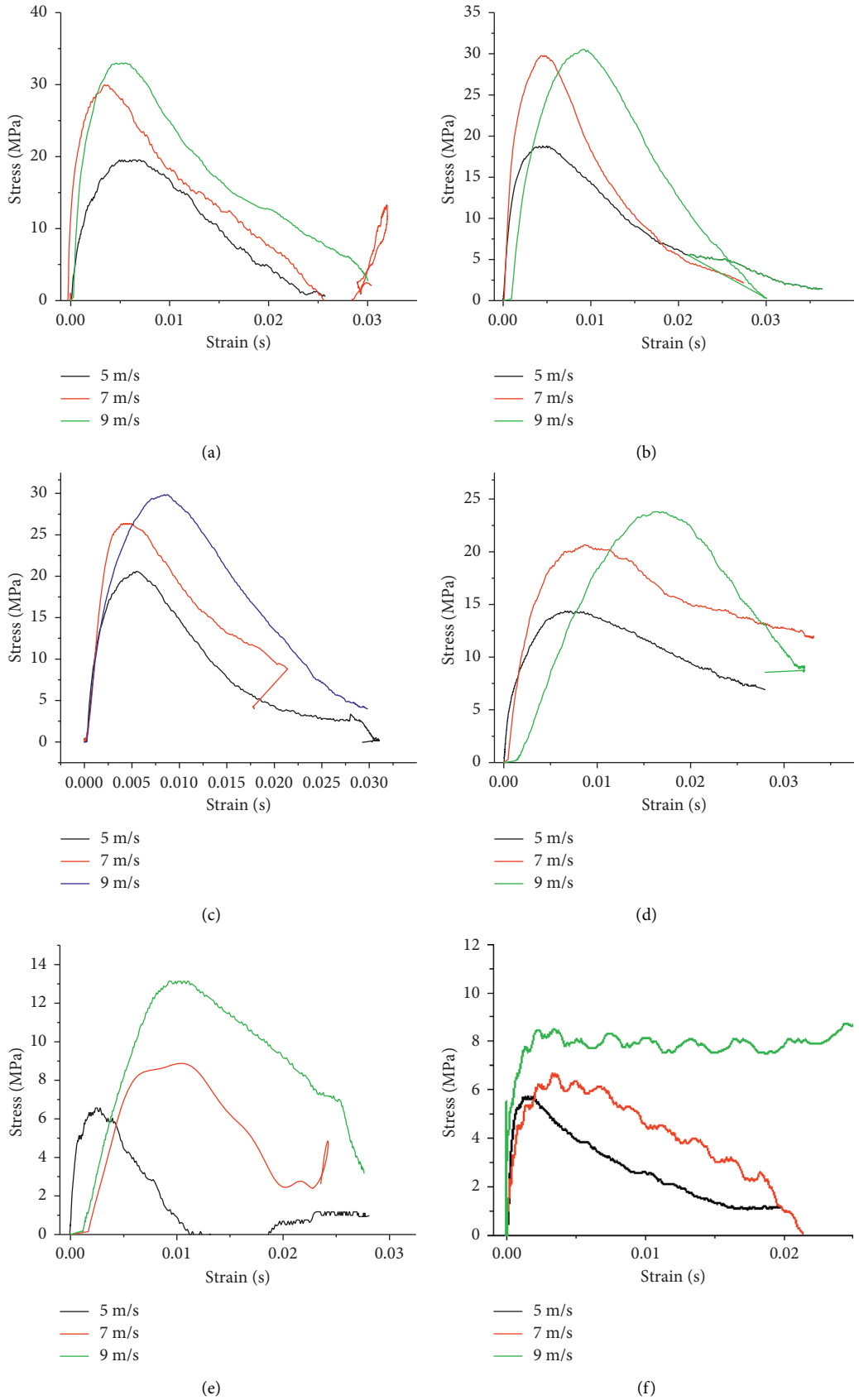

Figure 20: Stress-strain curves for the rock under different dynamic loads and temperature during dynamic BTS tests. (a) 25°C. (b) 100°C. (c) 200°C. (d) 400°C. (e) 600°C. (f) 800°C.

The stress-strain curves for the specimens under different loading rates and various temperatures are illustrated in Figure 20. For all the curves, they indicate that the impact speed of the bullet significantly influences the tensile strength of the rock. However, with the increase of the temperature, the tensile strength (peak stress) decreases. As can be seen in Figure 20(a), the peak strength is about 20 MPa at the impact speed of 5 m/s and room temperature, while it is only about 5.8 MPa (Figure 20(f)) at the same impact speed but under the temperature of 800°C. Thus, the temperature has an obvious influence on the tensile strength of the specimen. In addition, under the same temperature, for all the curves, the peak stress of the curve with a higher impact speed is much larger than that with a lower impact speed. Thus, the loading rate severely influences the tensile strength of the rock specimen.

6. Conclusions

This research has studied rock behaviour under the coupled dynamic loads and high temperatures. The SHPB system is used to carry out the test under different temperatures. The influences of the loading rate and the temperature are analysed. It is concluded that

(i) Under static loading, with the increase of temperature, the compressive strength of rock decreases. Before 400°C, the strength is not significantly influenced by the temperature, while after 400°C, the temperature plays a critical role in the rock strength under static loading.

(ii) Under the same impact velocity, the peak strength of marble decreases with the increase of temperature. However, with the increase of temperature, the peak strain of marble under high temperature increases. The dynamic elastic modulus of marble decreases with the increase of temperature, while the dynamic peak strength of marble decreases with the increase of temperature.

(iii) For the BTS test, the tensile strength increases with the increase of the loading rate. However, the tensile strength decreases with the increase of the temperature.

(iv) The failure modes of the dynamic BTS test are similar to those under static loading. The specimen is split into two halves along the loading diameter. Many fragments are produced at the top and bottom loading areas. With the increase of the loading rate, more fragments at the loading area are produced.

Data Availability

The data used to support the findings of this study are included within the article.

Conflicts of Interest

The authors declare that there are no conflicts of interest regarding the publication of this paper.

Acknowledgments

This work was partly supported by the National Science Foundation of China (Grant no. 11862010), Science and Research Fund from the Educational Department of Yunnan Province (Grant nos. 2020J0051 and KKJJ202067001); Research Start-Up Fund for Talent of Kunming University of Science and Technology (Grant no. KKSY201867017), and Program for Innovative Research Team (in Science and Technology) in University of Yunnan Province, and Yunnan Key Laboratory of Sino-German Blue Mining and Utilization of Special Underground Space, which are greatly appreciated.

References

[1] Z. Yin, W. Chen, H. Hao et al., "Dynamic compressive test of gas-containing coal using a modified split Hopkinson pressure bar system," *Rock Mechanics and Rock Engineering*, vol. 53, no. 2, pp. 815–829, 2020.

[2] J. Zhao, Y. X. Zhou, A. M. Hefny et al., "Rock dynamics research related to cavern development for ammunition storage," *Tunnelling and Underground Space Technology*, vol. 14, no. 4, pp. 513–526, 1999.

[3] Z.-Q. Yin, "Assessment of blasting-induced ground vibration in an open-pit mine under different rock properties," *Advances in Civil Engineering*, vol. 2018, Article ID 4603687, 10 pages, 2018.

[4] H. An, S. Hou, and L. Liu, "Experimental and numerical study of the concrete stress and fracture propagation processes by blast," *Engineering Letters*, vol. 27, no. 4, pp. 669–675, 2019.

[5] H. An and H. Liu, "Hybrid finite-discrete element modelling of dynamic fracture of rock and resultant fragment arching by rock blast," in *Proceedings of the ISRM International Symposium-8th Asian Rock Mechanics Symposium*, International Society for Rock Mechanics, Sapporo, Japan, October 2014.

[6] H. M. An, H. Y. Liu, H. Han, X. Zheng, and X. G. Wang, "Hybrid finite-discrete element modelling of dynamic fracture and resultant fragment casting and muck-piling by rock blast," *Computers and Geotechnics*, vol. 81, pp. 322–345, 2017.

[7] H. An, H. Liu, X. Wang, J. Shi, and H. Han, "Hybrid finite-discrete element modelling of blast-induced excavation damaged zone in the top-heading of deep tunnels," *Stavební Obzor—Civil Engineering Journal*, vol. 26, no. 1, pp. 22–33, 2017.

[8] H. An, "Hybrid continuum-discontinuum modelling of rock fracutre process in brazilian tensile strength test," *Civil Engineering Journal-Stavebni Obzor*, vol. 26, no. 3, pp. 237–249, 2017.

[9] H. M. An and L. Liu, "Numerical study of dynamic behaviors of concrete under various strain rates," *Archives of Civil Engineering*, vol. 65, no. 4, pp. 21–36, 2019.

[10] H. An, "Hybrid finite-discrete element method modelling of Brazilian disc tests," in *Proceedings of the International Conference on Civil, Transportation and Environment (ICCTE 2016)*, pp. 371–377, Guangzhou, China, January 2016.

[11] H. An, "Hybrid finite-discrete element method modeling of rock failure processes in Brazilian disc tests," *Electronic Journal of Geotechnical Engineering*, vol. 21, 2016.

[12] S. Jianjun and A. Huaming, "Simulation research on collapse vibration caused by demolition blasting," in *Proceedings of the 2013 Fourth International Conference on Digital*

Manufacturing and Automation (ICDMA), IEEE, Qingdao, China, June 2013.

[13] H. Liu and H. An, "Hybrid finite-discrete modelling of dynamic fracture of rock under impact loads and resultant fragment grinding," in *International Conference on Geomechanics, Geo-Energy and Geo-Resources (IC3G 2016)*, Melbourne, Australia, September 2016.

[14] H. Y. Liu, H. Han, H. M. An, and J. J. Shi, "Hybrid finite-discrete element modelling of asperity degradation and gouge grinding during direct shearing of rough rock joints," *International Journal of Coal Science & Technology*, vol. 3, no. 3, pp. 295–310, 2016.

[15] A. Kumar, "The effect of stress rate and temperature on the strength of basalt and granite," *Geophysics*, vol. 33, no. 3, pp. 501–510, 1968.

[16] Z. P. Bazant, S.-p. Bai, and R. Gettu, "Fracture of rock: effect of loading rate," *Engineering Fracture Mechanics*, vol. 45, no. 3, pp. 393–398, 1993.

[17] T. Blanton, "Effect of strain rates from 10-2 to 10 sec-1 in triaxial compression tests on three rocks," *International Journal of Rock Mechanics and Mining Sciences & Geomechanics Abstracts*, vol. 81, no. 1, pp. 47–62, 1981.

[18] G. Johnson, *Numerical Algorithms in a Lagrangian Hydrocode*, DTIC Document, Fort Belvoir, VA, USA, 1997.

[19] X. B. Li, T. S. Lok, and J. Zhao, "Dynamic characteristics of granite subjected to intermediate loading rate," *Rock Mechanics and Rock Engineering*, vol. 38, no. 1, pp. 21–39, 2005.

[20] H. Kolsky, "Stress waves in solids," Courier Corporation, Chelmsford, MA, USA, 1963.

[21] H. Kolsky, "An investigation of the mechanical properties of materials at very high rates of loading," *Proceedings of the Physical Society. Section B*, vol. 62, no. 11, pp. 676–700, 1949.

[22] H. Zhang, *Experimental research on Dispersion Behavior of BIg diameter SHPB*, Kunming Univeristy of Sceince and Technology (Sceicne Version), Kunming, China, 2010.

[23] S. K. Samanta, "Dynamic deformation of aluminium and copper at elevated temperatures," *Journal of the Mechanics and Physics of Solids*, vol. 19, no. 3, pp. 117–135, 1971.

[24] D. J. Frew, M. J. Forrestal, and W. Chen, "Pulse shaping techniques for testing brittle materials with a split Hopkinson pressure bar," *Experimental Mechanics*, vol. 42, no. 1, pp. 93–106, 2002.

[25] J. W. Tedesco, M. L. Hughes, and C. A. Ross, "Numerical simulation of high strain rate concrete compression tests," *Computers & Structures*, vol. 51, no. 1, pp. 65–77, 1994.

[26] F. Gálvez, J. Rodríguez, and V. Sánchez, "Tensile strength measurements of ceramic materials at high rates of strain," *Le Journal de Physique IV*, vol. 7, no. C3, pp. C3-151–C3-156, 1997.

[27] P. Sukontasukkul, P. Nimityongskul, and S. Mindess, "Effect of loading rate on damage of concrete," *Cement and Concrete Research*, vol. 34, no. 11, pp. 2127–2134, 2004.

[28] J. Zhao, "Applicability of Mohr-Coulomb and Hoek-Brown strength criteria to the dynamic strength of brittle rock," *International Journal of Rock Mechanics and Mining Sciences*, vol. 37, no. 7, pp. 1115–1121, 2000.

[29] Z. X. Zhang, S. Q. Kou, L. G. Jiang, and P.-A. Lindqvist, "Effects of loading rate on rock fracture: fracture characteristics and energy partitioning," *International Journal of Rock Mechanics and Mining Sciences*, vol. 37, no. 5, pp. 745–762, 2000.

[30] F. Dai, S. Huang, K. Xia, and Z. Tan, "Some fundamental issues in dynamic compression and tension tests of rocks using split Hopkinson pressure bar," *Rock Mechanics and Rock Engineering*, vol. 43, no. 6, pp. 657–666, 2010.

[31] F. Dai, K. Xia, H. Zheng, and Y. X. Wang, "Determination of dynamic rock mode-I fracture parameters using cracked chevron notched semi-circular bend specimen," *Engineering Fracture Mechanics*, vol. 78, no. 15, pp. 2633–2644, 2011.

[32] E. Eissa and A. Kazi, "Relation between static and dynamic Young's moduli of rocks," *International Journal of Rock Mechanics and Mining Sciences & Geomechanics Abstracts*, vol. 25, no. 6, pp. 479–482, 1988.

[33] B. Mahanta, A. Tripathy, V. Vishal, T. N. Singh, and P. G. Ranjith, "Effects of strain rate on fracture toughness and energy release rate of gas shales," *Engineering Geology*, vol. 218, pp. 39–49, 2017.

[34] Z. Zhang, *Laboratory Studies of Dynamic Rock Fracture and In-Situ Measurements of Cutter Forces for a Boring Machine*, CRC Press, Boca Raton, FL, USA, 2001.

[35] Q. Wang, W. Li, and X. Song, "A method for testing dynamic tensile strength and elastic modulus of rock materials using SHPB," *Pure and Applied Geophysics*, vol. 163, no. 5-6, pp. 1091–1100, 2006.

[36] Z. Zhou, X. Li, Y. Zou, Y. Jiang, and G. Li, "Dynamic Brazilian tests of granite under coupled static and dynamic loads," *Rock Mechanics and Rock Engineering*, vol. 47, no. 2, pp. 495–505, 2014.

[37] K. Peng, "Experimental and numerical evaluation of rock dynamic test with split-Hopkinson pressure bar," *Advances in Materials Science and Engineering*, vol. 2017, Article ID 2048591, 12 pages, 2017.

[38] I. Van der Molen, "The shift of the α-β transition temperature of quartz associated with the thermal expansion of granite at high pressure," *Tectonophysics*, vol. 73, no. 4, pp. 323–342, 1981.

[39] S. O. Heard, "Lipopolysaccharide-induced myocardial depression is not mediated by thromboxane a2," *Critical Care Medicine*, vol. 18, no. 4, p. S258, 1990.

[40] Z.-G. Yan, "Experimental study on longitudinal wave characteristics of tuff, granite and breccia after high temperature," *Yantu Gongcheng Xuebao (Chinese Journal of Geotechnical Engineering)*, vol. 28, no. 11, pp. 2010–2014, 2006.

[41] T. Fengchen, "Repair of below pairt nasal defec by auricular compound tissue flap," *Chinese Journal of Reparative and Reconstructive Surgery*, vol. 4, p. 4, 1990.

[42] H. Zhao and L. Chen, "Experimental study of thermal expansion property of limestone," *Rock and Soil Mechanics*, vol. 32, no. 6, pp. 1725–1730, 2011.

[43] L. Chen, "Experimental research on heat swelling power of sandstone and limestone," *Journal of China University of Mining & Technology*, vol. 37, no. 5, pp. 670–674, 2008.

[44] X. Li, "Study of dynamic properties of siltstone under coupling effects of temperature and pressure," *Chinese Journal of Rock Mechanics and Engineering*, vol. 29, no. 12, pp. 2377–2384, 2010.

[45] T. Yin, *Study on Dynamic Behavior of Rocks Considering Thermal Effect*, Central South University, Changsha, China, 2012.

[46] T.-b. Yin, "Energy dissipation of rock fracture under thermo-mechanical coupling and dynamic disturbances," *Chinese Journal of Rock Mechanics and Engineering*, vol. 32, no. 6, pp. 1197–1202, 2013.

[47] J. Xu and S. Liu, "Effect of impact velocity on dynamic mechanical behaviors of marble after high temperatures," *Chinese Journal of Geotechnical Engineering*, vol. 35, no. 5, pp. 879–883, 2013.

[48] S. Liu, "Experimental research on mechanical behaviors of marble after high temperatures subjected to impact loading," *Chinese Journal of Rock Mechanics and Engineering*, vol. 32, no. 2, pp. 273–280, 2013.

[49] T. Akazawa, "New test method for evaluating internal stress due to compression of concrete (the splitting tension test) (part 1)," *Journal of Japan Society of Civil Engineers*, vol. 29, pp. 777–787, 1943.

[50] F. Carneiro, "A new method to determine the tensile strength of concrete," in *Proceedings of the 5th Meeting of the Brazilian Association for Technical Rules*, Springer, Berlin, Germany, 1943.

[51] G. Hondros, "The evaluation of Poisson's ratio and the modulus of materials of a low tensile resistance by the Brazilian (indirect tensile) test with particular reference to concrete," *Australian Journal of Applied Science*, vol. 10, no. 3, pp. 243–268, 1959.

[52] W. C. Zhu and C. A. Tang, "Numerical simulation of Brazilian disk rock failure under static and dynamic loading," *International Journal of Rock Mechanics and Mining Sciences*, vol. 43, no. 2, pp. 236–252, 2006.

[53] D. Li and L. N. Y. Wong, "The Brazilian disc test for rock mechanics applications: review and new insights," *Rock Mechanics and Rock Engineering*, vol. 46, no. 2, pp. 269–287, 2013.

[54] S. Timoshenko and J. Goodier, *Theory of Elasticity*, McGraw-Hill, New York, NY, USA, 1970.

[55] D. Fukuda, "Development of a 3D hybrid finite-discrete element simulator based on GPGPU-parallelized computation for modelling rock fracturing under quasi-static and dynamic loading conditions," *Rock Mechanics and Rock Engineering*, vol. 53, no. 3, pp. 1072–1112, 2020.

[56] Q. B. Zhang and J. Zhao, "Determination of mechanical properties and full-field strain measurements of rock material under dynamic loads," *International Journal of Rock Mechanics and Mining Sciences*, vol. 60, pp. 423–439, 2013.